Electronic Supplementary Material (ESI) for Dalton Transactions.

Supplementary Materials

CO_2 Fixation by Dicopper(II) Complexes in A Hypodendate Framework of N_8O_2

Yi-Hsueh Ho, Mu-Chieh Chang, Kuo-Hsuan Yu, Yi-Hung Liu, Yu Wang, Yuan-Chung Cheng,* and Jwu-Ting Chen*

Department of Chemistry, National Taiwan University, Taipei 106, Taiwan

jtchen@ntu.edu.tw

Experimental section

Materials. Unless otherwise stated, all starting chemicals and solvents were analytically pure and used without further purification.

Caution! *Perchlorate salts are highly explosive, and should be handled with care and in small amounts.*[1]

Synthesis of bis((pyridin-2-yl)methyl)amine (4).[2] 2-(aminomethyl)pyridine (4.16 g, 38.5 mmol) and 2-pyridinecarboxaldehyde (4.15 g, 38.7 mmol) were dissolved in methanol (40 mL) and stirred at room temperature. After 2 h, the solution was cooled to 0°C and $NaBH_4$ (1.50 g, 39.7 mmol) was added in small portions. After the reaction was stirred for 12 h at room temperature, 50 mL of water was added and stirred for 1 h. The mixture was extracted with CH_2Cl_2 (6 × 20 mL). The mixture was dried over $MgSO_4$ and filtered. After solvent evaporated, the residue was purified by distillation under reduce pressure to obtain yellow oil at 180°C in 58% (4.5 g) yields. ^{1}H NMR (ppm, $CDCl_3$, 400 MHz): δ 8.54 (d, *J* = 4.4 Hz, 2H, Py *H*-6), 7.62 (td, *J* = 7.6, 1.2, 2H, Py *H*-4), 7.33 (d, *J* = 7.7 Hz, 2H, Py *H*-3), 7.13 (t, *J* = 6.1, 2H, Py *H*-5), 3.96 (s, 4H, PyCH_2N). ^{13}C NMR (ppm, $CDCl_3$, 100.625 MHz): δ 159.5 (Py *C*-2), 149.1 (Py *C*-6), 136.3 (Py *C*-4), 122.1 (Py *C*-3), 121.7 (Py *C*-5), 54.6 (Py*C*H_2N).

Synthesis of 3,3'-(piperazine-1,4,diyl)bis(1-chloropropan-2-ol) (5).[3] Epichlorohydrin (1.42 g, 15.3 mmol) was dissolved in methanol (20 mL) and piperazine (0.65 g, 7.6 mmol) was added under stirring at room temperature for 12 h. After evaporated solvent, the obtained compound was used for next step without purification. ^{1}H NMR (ppm, $CDCl_3$, 400 MHz): δ 3.93 (q, *J* = 6.1 Hz, 2H, $CH_2CHOHCH_2$), 3.58~3.50 (m, 4H, CH_2Cl), 2.72~2.64 (m, 4H, *H*-a), 2.55 (m, 4H, *H*-a), 2.44 (d, *J* = 6.2 Hz, 4H, NCH_2CHOH). ^{13}C NMR (ppm, $CDCl_3$, 100.625 MHz): δ 66.5(*C*HOH), 60.8 (*C*H_2Cl), 53.3 (N*C*H_2*C*H_2N), 47.0 (N*C*H_2CH).

Synthesis of 3,3'-(piperazine-1,4-diyl)bis(1-(bis(pyridin-2-ylmethyl)amino)propan-2-ol) (H_2L). To a solution of **$H_2$6-Cl** (7.7 mmol) in methanol (30 mL) was added **HPy^{Py}** (4.15 g, 20.8 mmol). The mixture stirred at 50°C for 48 h then added triethylamine (2.2 mL, 15.8 mmol) for 1 h. The mixture was extracted with CH_2Cl_2 (15 × 20 mL), then dried over $MgSO_4$ and the solvent was removed. The residue was washed by hexane (3 × 100 mL) to remove starting material to give **H_2L** (1.50 g, 2.5 mmol, 33% yield). ^{1}H NMR (ppm, $CDCl_3$, 400 MHz): δ 8.50 (d, *J* = 4.8 Hz, 4H, Py *H*-6), 7.57 (td, *J* = 7.6, 1.8, 4H, Py *H*-4), 7.33 (d, *J* = 7.8 Hz, 4H, Py *H*-3), 7.13 (dd, *J* = 7.4, 4.9, 4H, Py *H*-5), 3.94~3.83 (m, 2H, C*H*OH), 3.89 (AB, 8H, PyCH_2N), 2.73~2.55 (m, 4H, PyCH_2NCH_2CHOH), 2.58~2.38 (m, 8H, NCH_2CH_2N), 2.32~2.24 (m, 4H, NCH_2CHOH). ^{13}C NMR (ppm, $CDCl_3$, 100.625 MHz): δ 159.2 (Py *C*-2), 148.9 (Py *C*-6), 136.4 (Py *C*-4), 123.0 (Py *C*-3), 122.0 (Py *C*-5), 65.6 (*C*HOH), 62.3 (N*C*H_2CHOH), 60.6 (Py*C*H_2N), 59.4 (PyCH_2N*C*H_2CHOH), 53.3 (N*C*H_2*C*H_2N). HR-ESI-MS *m/z* calcd. for

$C_{34}H_{45}N_8O_2^+$: 597.3665 $[M+H]^+$, found: 597.3673 $[M+H]^+$.

Synthesis of $[(H_4L)Cu_2](ClO_4)_6$ (2). H_2L (48.3 mg, 0.162 mmol) and copper(II) perchlorate hexahydrate (60.6 mg, 0.164 mmol) were added into a acetionitrile solution (2 mL), and then $HClO_4$ was used to control pH value to 4, stirring for 10 min at room temperature. Crystals of X-ray quality were obtained in acetonitirile by slow diffusion of dichloromethane (73.0 mg, 88% yield). HR-ESI-MS *m/z* calcd. for $C_{34}H_{43}N_8O_{11}Cl_2Cu_3^+$: 1119.0198 $[M\text{-}ClO_4^-]^+$, found: 1119.0208 $[M\text{-}ClO_4^-]^+$. UV-VIS (λ_{max}, nm (ε, M^{-1} cm^{-1}); CH_3CN): 623 (152). Anal. Calcd. for $C_{34}H_{46}Cl_6Cu_2N_8O_{26}\cdot 8H_2O$: C, 27.84; H, 4.26; N, 7.64. Found: C, 27.70; H, 4.3; N, 7.60. Molar conductivity (ACN): 588 Ω^{-1} cm^2 mol^{-1}.

Synthesis of $[LCu_3(\mu_2\text{-}OH)](ClO_4)_3$ (1). To a solution of copper(II) perchlorate hexahydrate (0.084 g, 0.23 mmol) in CH_3CN (5 mL) was added to a CH_3CN of ligand **H_2L** (0.045 g, 0.075 mmol), the resulting blue solution was stirred for 10 min and then to it was added triethylamine (42 μL, 0.30 mmol) and the color was changed to dark green. After stirring for 10 min, the solution was recrystallized by using THF to get green powder of LCu_3 (0.065 g, 78%). HR-ESI-MS *m/z* calcd. for $C_{34}H_{43}N_8O_{11}Cl_2Cu_3^+$: 998.0316 $[M\text{-}ClO_4^-]^+$, found: 998.0325 $[M\text{-}ClO_4^-]^+$. UV-VIS (λ_{max}, nm (ε, M^{-1} cm^{-1}); CH_3CN): 697 (196); ca. 860 (184). Molar conductivity (ACN): 353 Ω^{-1} cm^2 mol^{-1}. Anal. Calcd. for $C_{34}H_{43}Cl_3Cu_3N_8O_{15}\cdot 4H_2O$: C, 34.82; H, 4.38; N, 9.55. Found: C, 35.18; H, 4.44; N, 9.12.

Synthesis of $[L_2Cu_8(\mu_4\text{-}CO_3)_2(\mu_2\text{-}OH)_2](ClO_4)_6$ (3). H_2L (39.3 mg, 0.066 mmol) and copper(II) perchlorate hexahydrate (122.5 mg, 0.331 mmol) were dissolved in 3 mL of acetonitrile. After stirring for 10 min, four equivalents of triethylamine was added to the solution and stirred for 10 min. The resulting solution was stirred at room temperature while 50 g solid carbon dioxide was slowly added over a period of 30 min. Then, the 20 mL of H_2O was used to precipitate blue powder of LCu_8 (22.3 mg, 0.00897 mmol) in 27% yield. HR-ESI-MS *m/z* calcd. for $C_{70}H_{83}Cl_3Cu_8N_{16}O_{24}^+$: 714.9807 $[M\text{-}3ClO_4^-]^{3+}$, found: 714.9802 $[M\text{-}3ClO_4^-]^{3+}$. UV-VIS (λ_{max}, nm (ε, M^{-1} cm^{-1}); CH_3CN): ca. 730 (527); 885 (705). IR (KBr, cm^{-1}): $\nu(ClO_4^-)$ 1089, 627; $\nu(CO_3^{2-})$ 1655, 1399.

$[LZnCu_2(\mu\text{-}OH)](ClO_4)_3$. H_2L (0.0551 g, 0.0923 mmol) was dissolved in 5 mL acetone, and copper(II) perchlorate hexahydrate (0.0684 g, 0.185 mmol) was then added to the solution. Then the blue solution was added two equivalents perchloric acid (60% in H_2O, 30μL). After stirring for 10 min, zinc(II) perchlorate hexahydrate (0.0344 g, 0.0923 mmol) was added to the solution. After stirring for 20 min, five equivalents triethylamine (66 μL, 0.475 mmol) was added to the solution and precipitated blue powder from the solution. After drying under vacuum, the product of $[LZnCu_2Zn(\mu\text{-}OH)](ClO_4)_3$ could be obtained in 33% yield (0.0365 g, 0.0308 mmol). HR-ESI-MS *m/z* calcd. for $C_{34}H_{43}N_8O_{11}Cl_2Cu_2Zn^+$: 999.0306 $[M\text{-}ClO_4^-]^+$, found: 999.0324 $[M\text{-}ClO_4^-]^+$. UV-VIS (λ_{max}, nm (ε, M^{-1} cm^{-1}); CH_3CN): 892 (228); 324 (2423). Molar conductivity (ACN): 387 Ω^{-1} cm^2 mol^{-1}.

Physical Measurements. UV-VIS spectra were measured on a HITACHI U-2900 spectrophotometer in the wavelength range of 1100-200 nm. Infrared spectral measurements were carried out using a Varian 640-IR spectrophotometer. Elementary analyses were performed using a Heraeus vairo III-NCSH. Conductivity measurements were done on a SUNTEX SC-110. ESI-MS and HR-ESI-MS spectra were done on a Waters micromass ZQ 4000 and were done on dual ionization ESCi (ESI/APCi) source options Waters LCT Premier XE (water Corp., Manchester, UK) respectively. The X-band ESR spectra were recorded on a Bruker EMX-10/12. The NMR spectra were recorded on a Bruker AVIII 400 MHz, DPX 400 MHz spectrophotometer. The NMR corresponding frequency for ^{13}C NMR spectra was 100.625 MHz. Values upfield of ^{1}H and ^{13}C data were given in ppm (δ) relative to tetramethylsilane in $CDCl_3$. All spectra were obtained at ambient temperature and pressure unless stated otherwise. Splitting patterns were designed as follow: s, singlet; d, doublet; dd, doublet of doublet; ddd, doublet of doublet of doublet; t, triplet; q, quartet; quin, quintet; m, multiplet; A/B, AB pattern. Oxidation and reduction potentials of all complexes were determined by cyclic voltammetry (CV) with a scan rate of 200 mV/s in MeCN solutions (1.0 mM). A glassy carbon electrode and a platinum wire were used as the working electrode and the counter electrode, respectively. All potentials were recorded versus the Ag/AgCl (saturated) reference electrode and calibrated with the ferrocene/ferrocenium redox couple. Oxidation and reduction CV were performed by using 0.1 M tetra-n-butylammonium hexafluorophosphate ($TBAPF_6$) in MeCN as the supporting electrolyte.

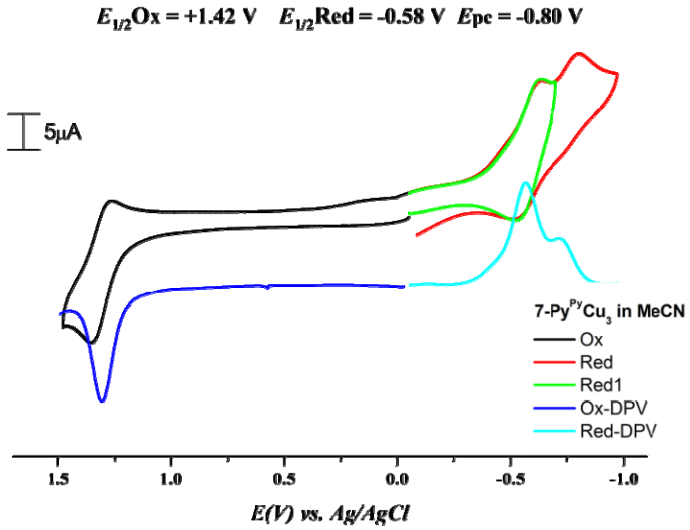

Figure S1. Cyclic voltammetry (black, red and green) and Differential-Pulse Voltammetry (deep and light blue) spectrum of **1** in acetonitrile containing $TBAPF_6$ (0.1 M) by using Ag/AgCl (saturated) as reference electrode at 25 ^{o}C.

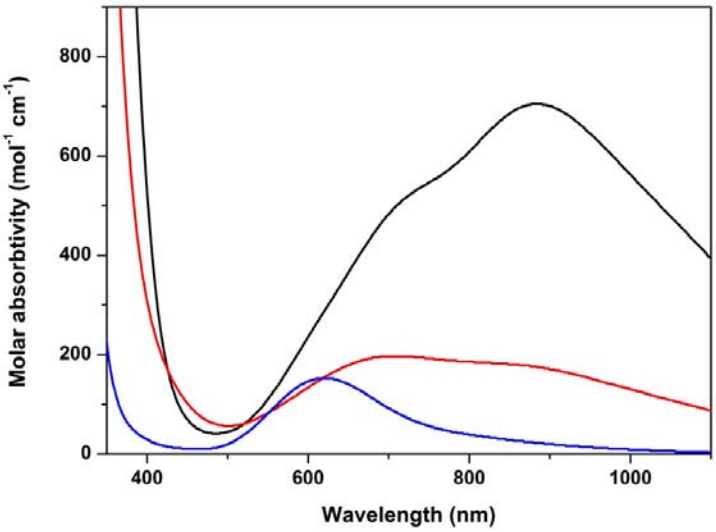

Figure S2. Electronic absorption spectra of **1** (red), **2** (blue) and **3** (black) in acetonitrile at 25 ^{o}C.

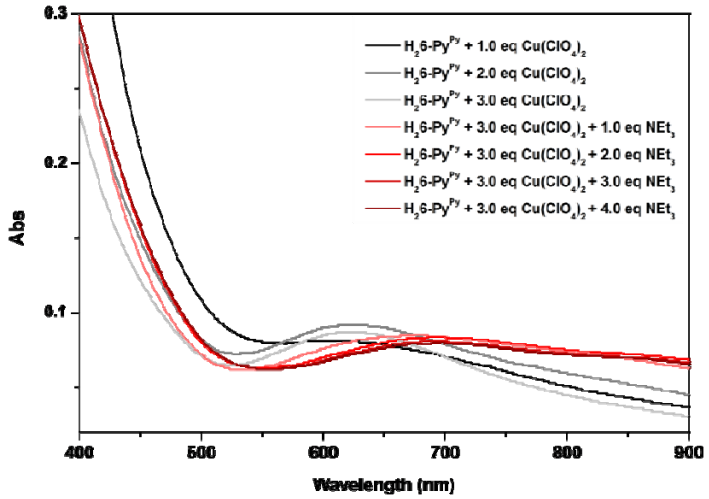

Figure S3. Electronic absorption spectra for the titration of $\mathbf{H_2L}$ (1.4×10^{-3} M) with $Cu(ClO_4)_2$ in acetonitrile at 25 ^{o}C (black to gray), and the generation of **1** after addition of triethylamine (pink to red).

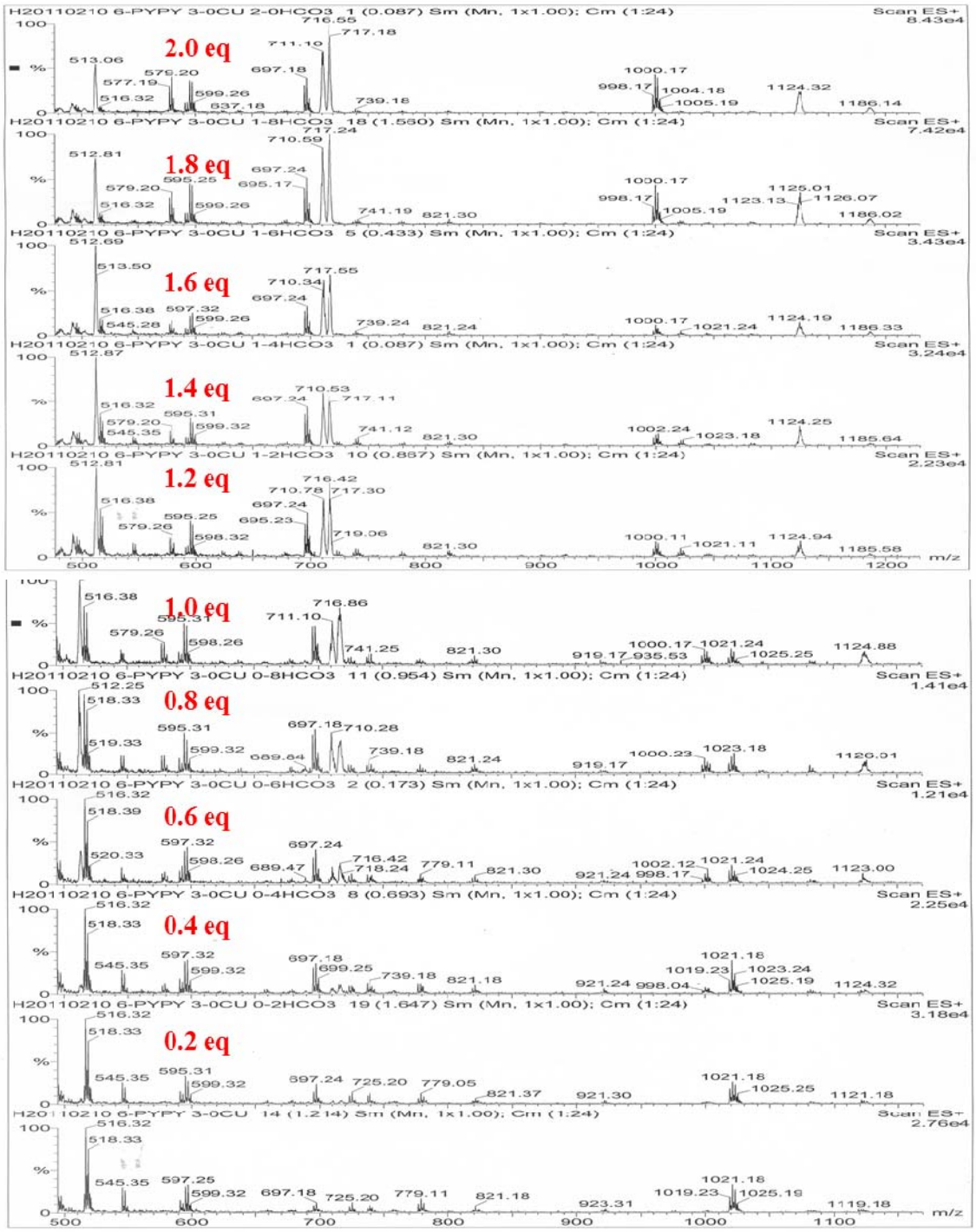

Figure S4. The ESI-MS spectra for the titration of the mixture of $\mathbf{H_2L}$ and three equivalents of $Cu(ClO_4)_2$ with $NaHCO_3$ in acetonitrile affording the complex **3**. (m/z = 1124 for $\mathbf{3}^{2+}$ $[(C_{34}H_{42}N_8O_2)_2Cu_8(CO_3)_2(OH)_2(ClO_4)_4]^{2+}$; m/z = 1000 $\mathbf{1}^{1+}$ $[(C_{34}H_{42}N_8O_2)Cu_3(OH)(ClO_4)_2]^{+}$; m/z = 1021 for $\mathbf{2}^{1+}$ $[(C_{34}H_{42}N_8O_2)Cu_2(ClO_4)_3]^{+}$, m/z = 512 for $\mathbf{3}^{4+}$ $[(C_{34}H_{42}N_8O_2)_2Cu_8(CO_3)_2(OH)_2(ClO_4)_2]^{4+}$; m/z = 716 for $\mathbf{3}^{3+}$ $[(C_{34}H_{42}N_8O_2)_2\ Cu_8(CO_3)_2(OH)_2(ClO_4)_3]^{3+}$. The other peaks might be impurity during this titration process, which were not observed in the spectrum of isolated complex **3**.)

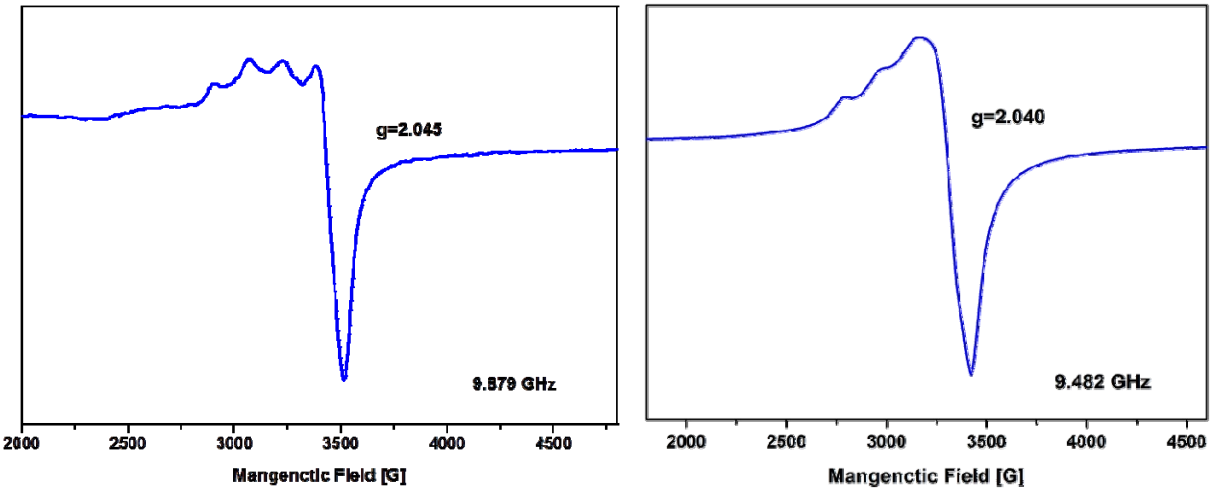

Figure S5. X-band EPR spectrum of **1** in solid state at 298 K(left) and 77 K(right).

Table S1. Summary of EPR data for **1**.

T	$g_{\|}$	$g_{\perp}$	$A_{\|}$	$A_{\perp}$
77 K	2.25	2.04	167	-
298 K	2.22	2.04	186	-

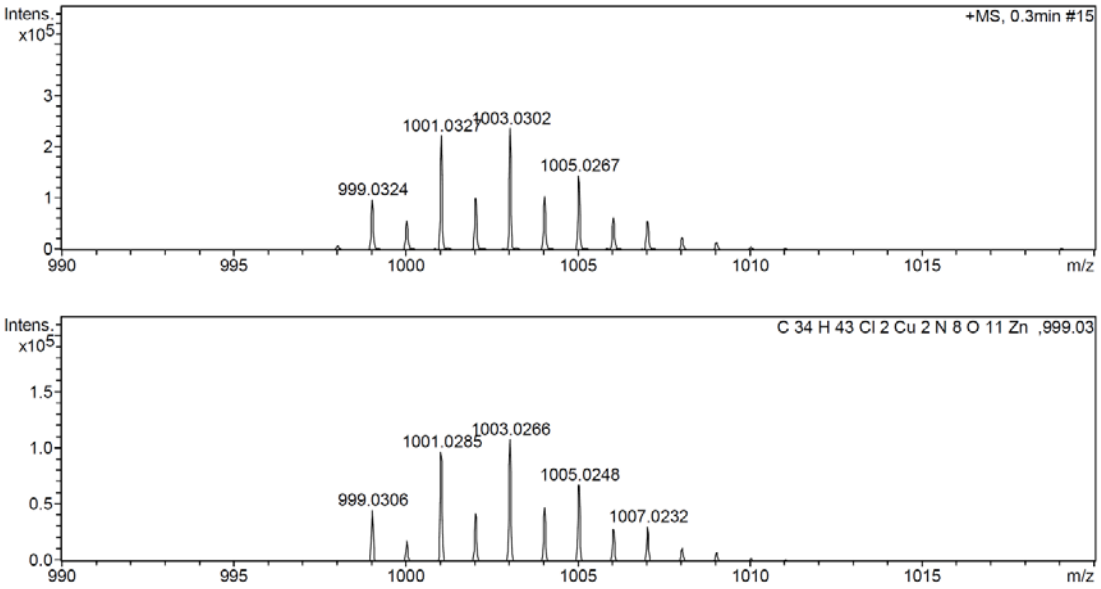

Figure S6. The HR-ESI-MS spectrum of $[LZnCu_2Zn(\mu\text{-}OH)](ClO_4)_3$ (top) and the simulated spectrum (bottom).

X-ray single crystal structure determination. Single crystals of suitable dimensions were used for data collection. Diffraction intensities were collected at 298 K on a Siemens SMART CCD XRD or Nonious CAD4 Kappa Axis XRD using graphite-monochromated Mo Kα radiation (λ = 0.71703 Å). The data were processed on a PC using the SHELXTL refinement software package.[4] The cell parameters for each structure were refined on F^2 by full matrix least-squares techniques. Hydrogen atoms were identified by calculation and refined using a riding mode, and their contributions to structure factors were included. Atomic scattering factors were taken from the International Tables of Crystallographic Data, Vol IV. Computing programs were from the NRcVAX package.[5]

Table S2. The structure parameters for **2** and **3**.

Complexes	**2**	**3**
formula	$C_{19}H_{32}Cl_3CuN_5O_{16}$	$C_{84}H_{96}C_{16}Cu_8N_{23}O_{36}$
M	756.39	2724.86
crystal system	Monoclinic	Triclinic
Space group	C2/c	P-1
a, Å	34.2225(6)	12.8818(3)
b, Å	8.2604(2)	14.6633(2)
c, Å	21.3491(4)	15.9762(4)
α, deg	90	72.159(10)
β, deg	100.531(2)	79.431(10)
γ, deg	90	75.616(2)
V, Å^3	5933.6(2)	2763.66(10)
Z	8	1
μ, nm^{-1}	1.088	1.746
R_1[a], wR_2[b] (I>2σ(I))	0.0469, 0.1313	0.0481, 0.1429

[a] $R_1 = \Sigma \, ||F_o| - |F_c|| \, / \, \Sigma \, |F_o|$. [b] $wR_2 = \{\Sigma \, [w(F_o^2 - F_c^2)^2 \, / \, (F_o^2)^2]\}^{1/2}$.

Computational Methods. Density functional calculations were performed by using the Gaussian 09 (G09) software package.[6] Calculations were performed in B3LYP functional.[7] Geometry optimization and frequency calculations were performed using the 6-31G* basis set.[8,9] Initial geometry optimizations were conducted on unrestricted states (S=3/2). The TD-DFT calculations were performed by using B3LYP/6-31G* with S=3/2 unrestricted states. The optimized structure of R,S-1 was utilized in the TD-DFT calculation which was more stable than R,R-1 isomer.

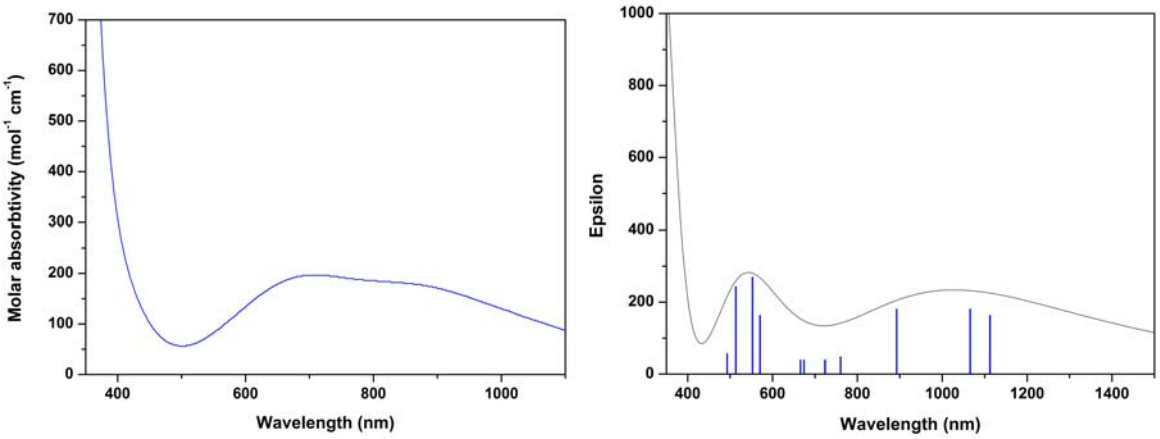

Figure S7. The experimental electronic spectrum data of compound **1** (left) and computational data (right), in which two sets of identified peaks were confirmed by TD-DFT calculation.

The calculated structure of $LZnCu_2$ is shown in **Figure S8**. The computational geometry of $LZnCu_2$, which is constituted with two trigonal bipyramidal (TBP) coordination centers on the bottom of the complex and one square planar zinc(II) center on the top N_2O_2 coordination site, is similar to compound **1**. Therein, the R,S-isomer is more stable around 0.6 kcal/mole than R,R-isomer. TD-DFT calculation is utilized to study the absorption spectrum in the range of *d-d* transition. Calculations are performed with the spin-unrestricted B3LYP functional with 6-31G* and spin state S =1.

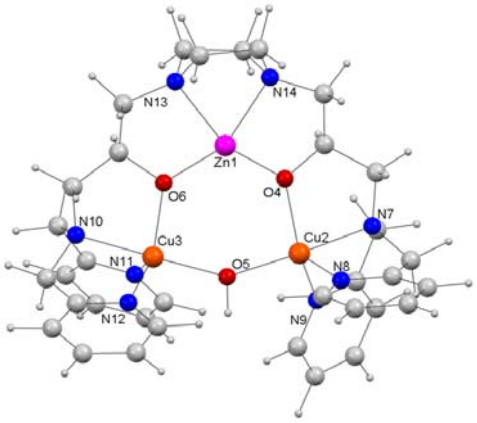

Figure S8 Calculated energy minimized geometries of the conformations R,S-LZnCu$_2$.

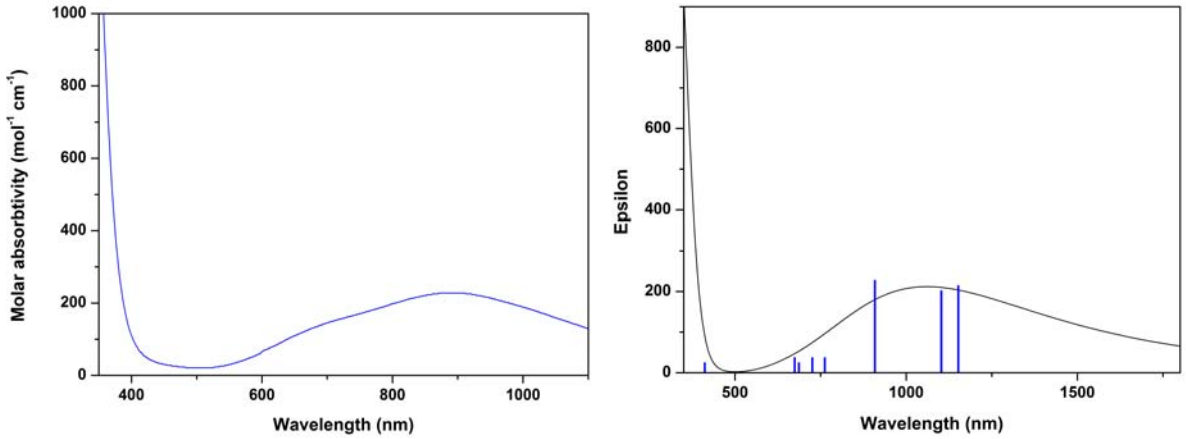

Figure S9. The experimental electronic spectrum data of mixed metal complex **[LZnCu$_2$(OH)](ClO$_4$)$_3$** (left) and computational data (right).

Magnetic Properties of 1

The plot of temperature dependence of the μ_{eff} is shown in **Figure S10**. At 350 K, the effective magnetic moment as 3.29 μ_B is slightly lower than the S = 3/2 ideal model system. The μ_{eff} values are decreased steadily with decreasing temperature. The value decays down to 1.63 μ_B at 5 K, which is lower than the value of ideal uncoupled spin S = 1/2. The curve shows an antiferromagnetic behavior both in high-temperature and low-temperature range, indicating this compound has some intermolecular spin interaction at low temperature range (5-25 K).[10]

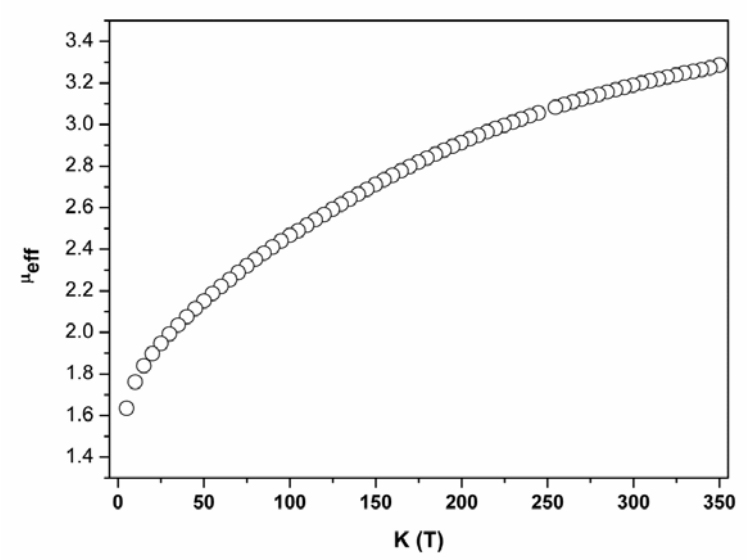

Figure S10. μ_{eff} (μ_B) vs. T experimental data for LCu_3 (○).

Magnetic Properties of 3

The magnetic susceptibility is measured in the temperature range 4–350 K, and **Figure S11** shows the plots of $\chi_M T$ versus T. At 350 K, the effective magnetic moment as 4.46 μ_B is slightly lower than the S = 2 ideal model system. Thus, the octanuclear copper complex could be taken as the combination of two tetracopper cluster system, and the maxium μ_B suggests that no interaction between such two tetracopper clusters. At room temperature, the χ_M for **3** is 2.49 cm^3 mol^{-1} K; it decreases continuously when the temperature decreases, and reaches a minimum value of 0.12 cm^3 mol^{-1} K at 4 K. Such magnetic behavior is characteristic phenomenon of a global antiferromagnetic interaction.

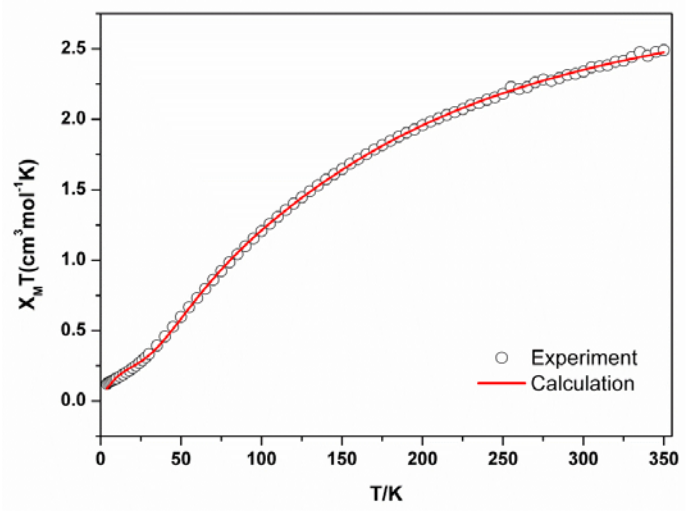

Figure S11. $\chi_M T$ vs. T experimental data for LCu_8 (○). Solid line shows the best fit obtained (see text).

The experimental data are fitted to the expression derived from the Hamiltonian $\hat{H} = -2J_{12}(\hat{S}_1\hat{S}_2) - 2J_{13}(\hat{S}_1\hat{S}_3 + \hat{S}_2\hat{S}_4) - 2J_{14}(\hat{S}_1\hat{S}_4 + \hat{S}_2\hat{S}_3) - 2J_{34}\hat{S}_3\hat{S}_4$, which corresponds to a tetranuclear spin center. The expression is also induced with a ρ paramagnetic impurity parameter in order to fit the low temperature data. The fitting equation, exchange interactions (J_{12}, J_{23}, J_{34} and J_{13}) and the atom labeling scheme are illustrated in **Scheme S1**. The most efficient superexchange pathway should be J_{12} base on the literature report through the oxo (from carbonate) bridge.[11] J_{34} corresponds to the interaction through an anti–anti carboxylate group. Also, J_{14} is the superexchange pathway through a carboxylate bridge in *syn–syn* fashion. Both J_{34} and J_{14} are expected to be antiferromagnetic behavior.[11a,11e]. The superexchange pathway occurs on J_{13} through an anti–syn configuration is possibly displayed ferromagnetic behavior in some literature report.[11d]

Scheme S1. The correlation diagram of the four magnetic coupling constants.

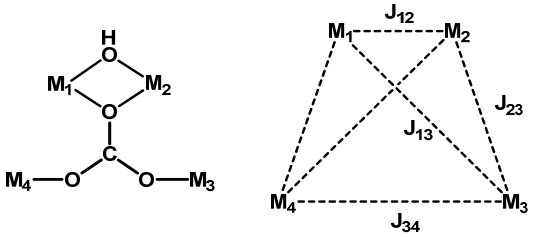

The parameter *g* is Landé factor and *ρ* is impurity parameter. The fitting parameters, using as a criterion of best fit the minimum value of $R = \sum(\chi_M^{Calc} - \chi_M^{Obs})^2 / \sum(\chi_M^{Obs})^2$. The best fit parameters are: J_{12} = -88.1 cm^{-1}, J_{34} = 1.1 cm^{-1}, J_{14} = -76.3 cm^{-1} and J_{13} = 33.0 cm^{-1} with g = 2.19, and R = 2.6 × 10^{-4}.

From the best fitting parameters, the most efficient superexchange pathway in **3** is corresponding to J_{12}, two copper atoms bridged by one carbonato oxygen atom and one hydroxide anion. The value of the J_{14} and J_{13} values are slightly sensitive to the shape or the maximum of the curve and their values are poorly determined, reflecting the difficulty of including six parameters in the regression analysis. However, the coupling constant of J_{12} is much smaller than other μ_4-CO_3 tetracopper(II) complexes. The magnetic interaction through the μ_2-η^2-O atom of the carbonate bridge can be ferro- or antiferromagnetic. The J_{12} seems to be ferromagnetic when the oxygen atom locates on apical position of copper center, such as $[Cu_6(bpy)_{10}(\mu\text{-}CO_3)_2(\mu\text{-}OH)_2](ClO_4)_6$.[11e] On the other hand, the antiferromagnetic should be observed when the oxygen atom occupies on equatorial position of the square planar or square pyramidal geometry of copper center. The antiferromagnetic coupling constant is affected by the angle of Cu-O-Cu angle. The larger antiferromagnetic coupling constant is resulted from the larger Cu-O-Cu angle, due to the better orbital overlapping through copper and oxygen. In the

cases of $[(\mu_4\text{-}CO_3)(\mu\text{-}Cl)_2\{Cu_4(bapa)_4\}]^{4+}$, $[(\mu_4\text{-}CO_3)(\mu\text{-}Cl)_2\{Cu_4(bapma)_4\}]^{4+}$ and $[(\mu_4\text{-}CO_3)(\mu\text{-}Cl)_2\{Cu_4(dpt)_4\}]^{4+}$ (bapa = bis(amino-propyl)amine; bapma = bis(aminopropyl)methylamine; dpt = bis(3-aminopropyl)-amine), the coupling constant of J_{12} are -390 cm^{-1}, -212 cm^{-1} and -121 cm^{-1} with the angle of Cu-O-Cu 129.3°, 124.0° and 121.0°, respectively. In the complex of **3**, the Cu-O-Cu angle as 93.8° is smaller than other μ_4-CO_3 copper containing compounds, which is expected with the smallest antiferromagnetic coupling constant with J_{12} = -88.1 cm^{-1}.

The value J_{12} is rational larger than J_{34}, because of the interaction just through one oxygen atom for J_{12} and through C-O-C (from carbonate) three atoms for J_{34}. Three types of coordination mode could cause different J_{34} values, which are described in **Table S3**. When the carbonate ligand bridges both copper atoms in a μ_2-η^1:η^1-O,O mode, the value of the magnetic interaction is usually small than J_{12}, and it can be ferro- or antiferromagnetic. When the coordination mode is in *syn-syn* fashion, the antiferromagnetic property is usually found in J_{34}. In addition, the ferromagnetic property is always found in *syn-anti* fashion, and the value is higher than 11 cm^{-1} as for the complexes of $[Cu(CO_3)(4\text{-}apy)_2]_n$.[11h] Nevertheless, **3** is the first compound that describes the J value in *anti-anti* carbonate coordination mode for Cu3 and Cu4, and the J value is higher than *syn-syn* but lower than *syn-anti* coordination modes, which a very small ferromagnetic coupling constant is found for J_{34} as 1.1 cm^{-1}. Moreover, the J_{23} (-76.3 cm^{-1}) is stronger than other μ_4-CO_3 complexes, because the J_{23} that through *syn-syn* mode of carbonate and one oxygen atom (from the alkoxide group) causes the larger spin orbital interaction than $[(\mu_4\text{-}CO_3)(\mu\text{-}Cl)_2\{Cu_4(bapa)_4\}]^{4+}$ (J_{23} = 22 cm^{-1}), $[(\mu_4\text{-}CO_3)(\mu\text{-}Cl)_2\{Cu_4(bapma)_4\}]^{4+}$ (J_{23} = -20 cm^{-1}) and $[(\mu_4\text{-}CO_3)(\mu\text{-}Cl)_2\{Cu_4\text{-}(dpt)_4\}]^{4+}$ (J_{23} = -58 cm^{-1}). The ferromagnetic property found in J_{13} for the complex **3** with the value as 44.9 cm^{-1} is larger than other μ_4-CO_3 complexes ($[(\mu_4\text{-}CO_3)(\mu\text{-}Cl)_2\{Cu_4(bapa)_4\}]^{4+}$, J_{13} = -10 cm^{-1}; $[(\mu_4\text{-}CO_3)(\mu\text{-}Cl)_2\{Cu_4(bapma)_4\}]^{4+}$, J_{13} = -72 cm^{-1}; $[(\mu_4\text{-}CO_3)(\mu\text{-}Cl)_2\{Cu_4\text{-}(dpt)_4\}]^{4+}$, J_{13} = 13 cm^{-1} and $[(Cu_2L)_2(CO_3)]$[11g], L = 2-(2-hydroxy-phenyl)-1,3-bis[4-(2-hydroxyphenyl)-3-azabut-3-enyl]-1,3-imidazolidine, J_{13} = -2.2 cm^{-1}), which is resulted from the *syn-anti* fashion of the carobonate coordination mode for J_{13}, but are *anti-anti* mode for the other complexes. In summary, the complex of **3** has smaller J_{12} and lager J_{23} due to the else bridged ligand of hydroxide and alkoxide respectively. On the other hand, the lager ferromagnetic coupling constant found in J_{13} is resulted from the *syn-anti* coordination mode of the carbonate with two copper ions. The *anti-anti* fashion of the J_{34} causes the weaker coupling constant for two copper ions, but still remains antiferromagnetic property.

Table S3 Carbonate complexes with similar coordination mode for **3**

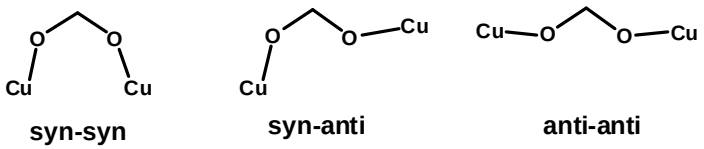

compound	J (cm^{-1})	type
$[Cu_6(bpy)(\mu\text{-}CO_3)_2(\mu\text{-}OH)_2](ClO_4)_6$ [11e]	2.75	syn-anti
$[Cu(CO_3)(4\text{-}apy)_2]_n$ [11h]	11	syn-anti
$[Cu_2(ascidH_2)(\mu\text{-}CO_3)(H_2O)_2]$ [11i]	1.6	syn-anti
$[Cu_4(bapa)_4(\mu_4\text{-}CO_3)(\mu\text{-}Br_2)]Br_4$ [11a]	-31	syn-syn
$[Cu_4(bapma)_4(\mu_4\text{-}CO_3)(\mu\text{-}Cl_2)]Cl_4$ [11a]	-26	syn-syn
$[Cu_4(dpt)_4(\mu_4\text{-}CO_3)(\mu\text{-}Cl_2)](ClO_4)_4$ [11f]	-22	syn-syn
3	1.1	anti-anti

bpy = 2,2'-bipirydine; 4-apy = 4-aminopyridine; $ascidH_2$ = ascidiacyclamide; bapa = bis(aminopropyl)-amine; bapma = bis(aminopropyl)methylamine; bis(3-aminopropyl)amine.

References

1 W. C. Wolsey, *J. Chem. Educ.* 1973, **50**, A335.

2 A. Neves, M. A. Brito, V. Drago, K. Griesar and W. Haase, *Inorg. Chim. Acta* 1995, **237**, 131.

3 P. P.-Y. Chen, R. B.-G. Yang, J. C.-M. Lee and S. I. Chan, *Proc. Natl. Acad. Sci. U.S.A.* 2007, **104**, 14570

4 G. M. Sheldrick, SHELXTL-97, *Program for Crystal Structure Solution*, University of Göttingen, Germany, 1997.

5 D. T. Cromer and J. T. Waber, , *International Tables for X-ray Crystallography*, The Kynoch Press, Birmingham, England, 1974, Vol. IV.

6 M. J. Frisch et al. Gaussian 09, Revision A.02; Gaussian, Inc.: Wallingford, CT, 2009.

7 A. D. Becke, *J. Chem. Phys.* 1993**, 98**, 5648.

8 V. Rassolov, J. A. Pople, M. Ratner, P. C. Redfern and L. A. Curtiss, *J. Comput. Chem.* 2001, **22**, 976.

9 V. A. Rassolov, J. A. Pople, M. Ratner, T. L. Windus, *J. Chem. Phys.* 1998, **109**, 1223.

10 I. Gautier-Luneau, D. Phanon, C. Duboc, D. Luneau and J.-L. Pierre, *Dalton Trans.* 2005, 3795; B. N. Figgis and D. J. Martin, *J. Chem. Soc., Dalton Trans.* 1972, 2174; E. Y. Tsui, M. W. Day and T. Agapie, *Angew. Chem., Int. Ed.* 2011, **50**, 1688; V. H. Crawford, H. W. Richardson, J. R. Wasson,

D. J. Hodgson and W. E. Hatfield, *Inorg. Chem.* 1976, **15**, 2107; E. Ruiz, P. Alemany, S. Alvarez and J. Cano, *J. Am. Chem. Soc.* 1997, **119**, 1297.

11 A. Escuer, E. Peñalba, R. Vicente, X. Solans and M. Font-Bardía, *J. Chem. Soc., Dalton Trans.* 1997, 2315; P.; Meester, S. R. Fletcher and S A. C. Kapsky, *J. Chem. Soc., Dalton Trans.* 1973, 2575; H. U. Gudel, A. Stebler and A. Furrer, *Inorg. Chem.* 1979, **18**, 1021; B. Chiari, O. Piovesana, T. Tarantelli and P. F. Zanazzi, *Inorg. Chem.* 1993, **32**, 4834; P. E. Kruger, G. D. Fallon, B. Moubaraki, K. J. Berry and K. S. Murray, *Inorg. Chem.* 1995, **34**, 4808; M. Rodríguez, A. Llobet, M. Corbella and P. Müller, *J. Chem. Soc., Dalton Trans.* 2002, 2900; M. Fondo, A. M. García-Deibe, M. Corbella, E. Ruiz, J. Tercero, J. Sanmartín and M. R. Bermejo, *Inorg. Chem.* 2005, **44**, 5011; J. Sertucha, A. Luque, P. Román, F. Lloret and M. Julve, *Inorg. Chem. Commun.* 1999, **2**, 14; A. L. Brenk, K. A. Byriel, D. P. Fairlie, R. L. Gahan, G. R. Hanson, C. J. Hawkins, A. Jones, C. H. L. Kennard, B. Moubaraki and K. S. Murray, *Inorg. Chem.* 1994, **33**, 3549.